Supplementary Information

Supplementary Methods

GRACE trends, and hydrology and GIA models

Fig. S1a shows the secular trend in surface mass determined from GRACE, smoothed using a 350 km radius Gaussian function[30]. Large negative trends are especially evident over Greenland, Alaska, and portions of the Antarctic coastline. Prominent positive trends occur over Canada, Scandinavia, and the Antarctic interior. GRACE has no vertical resolution, and so the Fig. S1a results do not distinguish between ice/snow/water on the surface, water stored in the ground, and changes within the solid Earth.

We use models to remove hydrological and solid Earth contributions. For hydrology, we use the average of two land surface models: the Community Land Model version 4.0 (CLM4)[31] (http://www.cesm.ucar.edu/models/ccsm4.0/clm/) and GLDAS/NOAH 2.7.1[32] (http://disc.sci.gsfc.nasa.gov/hydrology/index.shtml). Both models provide global, monthly soil moisture and snow estimates, and CLM4 includes non-anthropogenic groundwater variations. For each model there are a few locations, usually in glacierized areas, where the predicted water storage increases at unrealistically high rates. We zero out those locations before removing them from the GRACE results. The atmospheric forcing dataset used in GLDAS/NOAH is NCEP/NCAR Reanalysis 1 (ref. [33]), whereas CLM4 was forced with CRUNCEP

(http://dods.extra.cea.fr/data/p529viov/cruncep/readme.htm).

Fig. S1b shows the GRACE results after subtracting both the average of the two hydrology models, and a model of Glacial Isostatic Adjustment (GIA): the Earth's viscoelastic response to the removal of ice following the last ice age. The GIA model

(results computed and provided by Geruo A) uses the ICE5G deglaciation history and VM2 viscosity profile[34]. It assumes a compressible Earth, and includes polar wander feedback, degree-one terms, and a self-consistent ocean. Subtracting the GIA model removes the positive trends over Canada, Scandinavia, and the Antarctic interior (Fig. S1b). Though the GIA model within Antarctica is only loosely constrained because the ice history there is poorly known.

Fig. S1c shows the residual mass trend after removing the results of the mascon inversion. Large negative trends over major ice-covered regions have become close to null in Fig. S1c, indicating the ability of the inversion to capture ice loss.

Mascon fitting

Mascons are user-defined regions of the Earth's surface, chosen here so that together they span every region that has a concentrated glacier area greater than 100 km^2, as well as the plains of northern India, Pakistan, and Bangladesh where there are large GRACE trends adjacent to glacierized regions. Each mascon is composed of many small blocks, where the block centers are defined on a 0.5 degree grid. Thus, the mascons do not exactly match the surface area of the glacierized regions they cover. This has no effect on the mascon solution, as long as the glaciated region is within the mascon, because GRACE senses the total mass change. The mascons are available online as a shapefile.

We exclude small glacier systems that have sub 100 km^2 areas, and that are also isolated from all other glacier systems, based on ref. [2]. For example, all African glaciers and some Russian glacier systems are excluded. The rationale for omitting those regions, besides the simple fact that they are small, is that the mass loss estimates for those

systems from ref. [2] are all negligible (so that our decision to omit mascons that cover those systems is not likely to have any significant impact on our global results), and that since they are surrounded by large non-glaciated regions, our estimates for those systems might be particularly susceptible to hydrology model errors.

We follow the procedure described in ref. [17], and fit mascon amplitudes to the GRACE Stokes coefficients to obtain estimates of the monthly mass variability of each mascon. For each mascon, we find the set of Stokes coefficients that would be caused by a unit mass distributed uniformly over that mascon. Let the degree l, order m Stokes coefficients for mascon i be (C_{lm}^i, S_{lm}^i). Let the actual, but unknown, mass of mascon i be M_i. We estimate the M_i's for all the mascons by fitting them simultaneously to the GRACE monthly Stokes coefficients. Before fitting, we apply a 150-km Gaussian smoothing function to the Stokes coefficients: both to the GRACE coefficients, and to the coefficients for each mascon. We do this to reduce the noise in the monthly M_i time series; though we have found that the trend estimates we obtain without applying this smoothing function are almost the same as those shown in Table 1.

Let $\left(\Delta C_{lm}(t), \Delta S_{lm}(t)\right)$ be the GRACE coefficients at time t, after removing the mean of all the monthly solutions (and after removing the hydrology and GIA models, as described above). The mean must be removed, because otherwise contributions from the Earth's interior, which dominate the mean signal, would be misinterpreted as surface mass signals. As a result, GRACE can be used to determine change of ice mass, but not total ice mass.

Before fitting, the GRACE and mascon Stokes coefficients are multiplied by $W_l(2l+1)/(1+k_l)$, where W_l are the coefficients of the Gaussian smoothing function, and

the k_l are load Love numbers to transform these geoid coefficients into smoothed spherical harmonic coefficients of mass [see ref.[30]]. We denote these modified Stokes coefficients with asterisks (i.e. $C_{lm}^{*,i}$, etc.), and find the $\{M_i(t)\}$ that minimize the standard least-squares merit function:

$$E = \sum_{l,m}\left[\left(\Delta C_{lm}^*(t) - \sum_i C_{lm}^{*,i} M_i(t)\right)^2 + \left(\Delta S_{lm}^*(t) - \sum_i S_{lm}^{*,i} M_i(t)\right)^2\right] \qquad (A1)$$

for each monthly time step, t. The $\{M_i(t)\}$ that minimize (A1) solve

$$Y_j(t) = \sum_i B_{ji} M_i(t) \qquad (A2)$$

where

$$Y_j(t) = \sum_{lm}\left(\Delta C_{lm}^*(t) C_{lm}^{*,j} + \Delta S_{lm}^*(t) S_{lm}^{*,j}\right) \qquad (A3)$$

$$B_{ji} = \sum_{lm}\left(C_{lm}^{*,j} C_{lm}^{*,i} + S_{lm}^{*,j} S_{lm}^{*,i}\right) \qquad (A4)$$

The solution to (A2) is

$$M_i(t) = \sum_j B_{ij}^{-1} Y_j(t) \qquad . \qquad (A5)$$

This procedure differs somewhat from that described in ref. [17], in that ref. [17] applied a destriping filter to the GRACE Stokes coefficients and to the mascon Stokes coefficients, before fitting. We have elected to omit this filter. This results in noisier monthly time series, but improves the sampling characteristics of our sensitivity kernels (see the next section).

Sensitivity kernels

Ideally, the solution for $M_i(t)$ would recover the true spatial average of mascon i's mass: i.e. a spatial average that samples every point inside the mascon with a sensitivity of 1, and every point outside with a sensitivity of 0. Unfortunately, because of the finite number of harmonic degrees in the GRACE solution (l_{max}=60 for CSR solutions), this is not the case. It is possible to determine the sensitivity kernel of each mascon solution, which not only provides insight into possible biases in those solutions but can help when deciding how to choose mascon sizes, shapes, and locations.

Let $\Delta\sigma(\theta,\phi,t)$ be the surface mass at co-latitude θ, longitude ϕ, and time t. Because the inverted mascon masses, M_i, are linearly related to the GRACE coefficients (through (A5)), and those coefficients are linearly related to $\Delta\sigma(\theta,\phi,t)$ (through Newton's Law of Gravity), there must be a linear relation between each M_i and $\Delta\sigma(\theta,\phi,t)$. The most general linear relation has the form

$$M_i(t) = \int \Delta\sigma(\theta,\phi,t)\, A_i(\theta,\phi)\, a^2 \sin\theta\, d\theta\, d\phi \qquad\qquad (A6)$$

where $A_i(\theta,\phi)$ is the sensitivity kernel for mascon i, and would ideally equal 1 for points inside the mascon and 0 outside, and a is the mean radius of the Earth.

To discover what $A_i(\theta,\phi)$ actually is, note that (A3)-(A5) imply a linear relation between M_i and the GRACE Stokes coefficients:

$$M_i(t) = \sum_{lm}\left[A_{lm}^{C,i}\Delta C_{lm}(t) + A_{lm}^{S,i}\Delta S_{lm}(t) \right] \qquad , \qquad\qquad (A7)$$

where the factors $A_{lm}^{C,i}$, $A_{lm}^{S,i}$ can be determined as described below. The relation between the Stokes coefficients and $\Delta\sigma(\theta,\phi,t)$, implied by Newton's Law of Gravity, is [see ref.[30]].

$$\begin{bmatrix} \Delta C_{lm}(t) \\ \Delta S_{lm}(t) \end{bmatrix} = \frac{3(1+k_l)}{4\pi\rho_{ave}a^3(2l+1)} \int \Delta\sigma(\theta,\phi,t) P_{lm}(\cos\theta) \begin{Bmatrix} \cos m\phi \\ \sin m\phi \end{Bmatrix} a^2 \sin\theta \, d\theta \, d\phi \quad (A8)$$

where the $P_{lm}(\cos\theta)$ are Associated Legendre functions, and ρ_{ave} is the Earth's mean density. Putting (A8) into (A7) gives

$$M_i(t) = \int \Delta\sigma(\theta,\phi,t) a^2 \sin\theta \, d\theta \, d\phi \sum_{lm} \frac{3(1+k_l)}{4\pi\rho_{ave}a^3(2l+1)} P_{lm}(\cos\theta) \left(A_{lm}^{C,i} \cos m\phi + A_{lm}^{S,i} \sin m\phi \right)$$

This is of the form (A6), where the sensitivity kernel is

$$A_i(\theta,\phi) = \sum_{lm} P_{lm}(\cos\theta) \left(A_{lm}^{C,i} \cos m\phi + A_{lm}^{S,i} \sin m\phi \right) \frac{3(1+k_l)}{4\pi\rho_{ave}a^3(2l+1)} \quad . \quad (A9)$$

The sensitivity kernel can thus be determined from knowledge of $A_{lm}^{C,i}$ and $A_{lm}^{S,i}$. Those factors can be found numerically, as follows. Define a synthetic set of Stokes coefficients, where $\Delta C_{l'm'} = 1$ for a single (l', m'), and all other Stokes coefficients are 0. Apply the fitting procedure described in (A3)-(A5) to this simple set of Stokes coefficients. From (A7) we know the result for M_i will equal $A_{l'm'}^{C,i}$. Repeating this for each (l', m'), and then for the $\Delta S_{l'm'}$'s as well, yields every $A_{l'm'}^{C,i}$ and $A_{l'm'}^{S,i}$, one at a time, which can then be put into (A9) to obtain the sensitivity kernel. These steps can be repeated for every mascon i.

We have subdivided some of the ice-covered regions into more than one mascon (see below, for an explanation). For each of those regions, the results for those mascons are summed to obtain the Table 1 entry, and the sensitivity kernel for that entry is the sum of the sensitivity kernels for each of the contributing mascons.

It can be shown that the mascon sensitivity kernels have the following useful property. Let i and j represent any two mascons used in a simultaneous mascon fit, and let $A_i(\theta,\phi)$ be the sensitivity kernel for mascon i. Then

$$\frac{1}{S_j} \int_{S_j} A_i(\theta,\phi) \sin\theta \, d\theta \, d\varphi = \delta_{ij} \qquad , \qquad (A10)$$

where S_j is the surface area of mascon j : i.e the area-averaged sensitivity kernel of a mascon is 1 over itself and 0 over any other mascon used in the simultaneous inversion. This implies that if a mass anomaly is distributed uniformly across a mascon, the solution for that mascon will deliver the true mascon average, and that this mass anomaly will not contaminate the solution for any other mascon. Thus, if there's reason to believe there is a significant, non-ice mass anomaly close to an ice-covered region, (A10) suggests it would be prudent to cover that anomaly with mascons to minimize leakage into the ice-covered mascon estimates. That is why we placed mascons over the plains of northern India, Pakistan, and Bangladesh.

If the non-ice anomaly is not uniform across one or more of its mascons, that anomaly could still cause leakage into the adjacent ice mascon solutions. The result (A10) suggests that increasing the number of mascons covering the anomaly could reduce this leakage, so that the anomaly is more nearly constant across each individual mascon. The same

argument holds for an ice-covered region: if that region is covered with more mascons, each mascon solution will better represent the true average over that mascon. The drawback of using more and smaller mascons, is that then the inversion relies more on the higher harmonic degrees (i.e. shorter spatial scales) to separate them. And, because GRACE does not determine higher harmonics as accurately, this can degrade the accuracies of the mascon solutions.

As an example of an averaging kernel, Fig. S2 shows the sum of all sensitivity kernels for all mascons shown in Fig. 1. Fig. S3a and b show the kernel for HMA and the kernel for the adjacent plains, computed for the mascon distribution shown in the figure and used to generate the Table 1 values. The kernel is the sum of the sensitivity kernels for all the individual mascons in each of those regions. Note that the two kernels are well-localized to their respective regions.

We assessed the likely impact of leakage from the India plains groundwater signal, by convolving the sensitivity kernel for the HMA mascons (Figure S3a) with the GRACE mass trend over the India plains mascons. This leakage equates to less than 1 Gt/yr.

Little Ice Age Model.

Ongoing solid Earth deformation induced by the addition and subsequent removal of ice at the start and end of the Little Ice Age (LIA) would cause a present-day positive gravity trend across each glaciated region. If these trends are not removed from the GRACE results, they could cause us to underestimate the present-day ice loss in those regions. LIA corrections for Alaska and Patagonia are taken from previous work (see the

main text). For the other GIC regions, we construct a viscoelastic GIA model and use it with plausible but extreme LIA and viscoelastic parameter values, to obtain an upper bound for the LIA contributions in each region.

The GIA model, similar to that described in ref. [35], assumes an incompressible, self-gravitating Earth, consisting of an elastic lithosphere, an inviscid fluid core, and a viscoelastic mantle. We model each glacier system as a uniform disc with an area equal to the area of the glaciated region. We assume a steady glaciation phase between 1550 and 1710 AD, followed by a period of stability, and a subsequent steady deglaciation phase between 1850 and 2000 AD. This is a more recent LIA deglaciation period than is likely for most glaciated regions[36], but is chosen here to obtain an upper bound for the LIA contributions. The ice volume added during glaciation is assumed to be equal to that subtracted during deglaciation. To estimate that volume, we use the 1961-2006 ice loss rates described in ref. [2], and assume those rates are appropriate for the entire 1850-2000 period. This is a tenuous assumption, because the actual LIA deglaciation rates could well have been significantly different than the rates inferred for the last half of the 20'th century. Furthermore, ref. [2] shows large 1961-2006 ice loss rates for HMA (47 km^3/yr) and for North America outside Alaska, (27 km^3/yr), whereas our 2003-2010 GRACE results for those same regions are not significantly different than zero. These differences between GRACE and ref. [2] could reflect a time-dependence in the mass loss rates. But that seems unlikely since ref. [2] 's 2002-2006 rates for those regions are even larger than these estimated earlier rates, and that latter time period overlaps ours. Still, we have elected to use the large ref. [2] ice loss rates for those regions to obtain upper bounds for the LIA contributions.

For the viscosity profile, we consider two cases. For regions near divergent or convergent plate boundaries (eg. HMA, the Alps, Iceland, Kamchatka, the Andes) we adopt a model similar to that assumed in ref. [29] for Patagonia: a 65 km thick lithosphere; and asthenospheric, upper mantle, and lower mantle viscosities of 1×10^{19} , 3×10^{20} , and 2.4×10^{21} Pa-sec , respectively. For more stable regions (eg. Ellesmere and Baffin Islands, Svalbard and the other Arctic Ocean archipelagos, Norway, North America outside Alaska), we adopt a profile similar to model VM2[34]: a 90-km thick lithosphere, with upper mantle and lower mantle viscosities of 9×10^{20} and 3.6×10^{21} Pa-sec, respectively.

We find that the only GIC region (other than Alaska and Patagonia) where the predicted GRACE correction is 1 Gt/yr or more, is HMA, where the model results suggest we remove 5 Gt/yr from the GRACE estimates. Because, for the reasons given above, our estimated LIA correction for this region is likely to be an overestimate, we interpret this result as indicating the true LIA signal is somewhere between 0 and 5 Gt/yr, and represent it as a 2.5 ± 2.5 Gt/yr signal.

Mass balance rates and uncertainties

To obtain the mass balance rates for each region shown in Table 1, we fit the Stokes coefficients (SC) of the mascons (shown in Figure 1) to (i) the SC of GRACE only, (ii) the SC of the GIA model and (iii) the SC of the two hydrology models. For steps (i) and (iii), we obtain time series of mass for each mascon, whereas step (ii) yields a single GIA correction value for each mascon's trend (GIA effects are linear in time). For each estimate shown in Table 1, whether it be a single region, or the entire GIC estimate, or the entire GIC+ Greenland+Antarctic estimate, we sum the inverted mass time series of

all mascons that comprise the region of interest, for the three cases defined above. Rates and uncertainties are then obtained from the resulting time series.

For (i), we least-squares fit a constant, trend, and annual and semi annual signals to the aggregate time series, after excluding 3 sigma outliers. We choose the uncertainty of the uncorrected GRACE trend to be the 2-sigma value obtained from the regression analysis of the trend estimate.

For (ii), we define the uncertainty as ±50% of the GIA signal, to which we quadratically add 50% of the LIA signal. This is equivalent to assuming the widths of the GIA/LIA uncertainty intervals are equal to the GIA/LIA corrections themselves.

For (iii), we fit a constant, trend and annual and semi-annual signals to the two aggregate time series – one for each land surface model. We choose the hydrology correction to be the average of the trends from the two hydrology models; and we define its uncertainty as ± the absolute difference between those two trends (so that the total uncertainty interval for the hydrology correction is twice the difference between the two model trends). 3 sigma outliers defined in (i) are here excluded in (iii) for consistency.

The final mass balance rate for any given region is

$mb = mb_{GRACE} - mb_{GIA} - mb_{LIA} - mb_{\text{hydrology}}$. The values of each individual term in this equation are shown in supplementary Table 1 for each region, with the three last terms on the right hand side multiplied by -1 so that they represent a correction that we add to the "GRACE only" values to obtain the "Mass balance rates".

The uncertainty is the quadratic sum of the uncertainties for (i), (ii) and (iii), defined above.

Thus, the uncertainties for the GRACE, GIA and hydrology components of the mass balance of the global GIC-excluding-PGIC rates (and, in fact, the uncertainty of every other multi-mascon region) are obtained by first summing the inverted time series of all of its constitutive mascons, and then estimating the error from the aggregate time series; instead of, for example, quadratically combining the uncertainties obtained from individual time series or constants of each constitutive mascon. This avoids any implicit assumption that errors in neighboring mascons are uncorrelated.

The hydrology correction is largest for the High Mountain Asia region (table S1), and equates to 16±17 Gt/yr. In this case, GLDAS/NOAH predicts a 7 Gt/yr correction, whereas CLM4 predicts a 24 Gt/yr correction. This discrepancy between the two models is the largest contributor to the uncertainty of the HMA rate estimate, and it is reflected in the relatively large ±20 uncertainty of the Table 1 HMA estimate.

Influence of inter-annual variability and study duration

The GRACE estimates in this study reflect the mass balance over only the last 8 calendar years (2003-2010). The possibility of multi-year or decadal-scale variability suggests caution if trying to extend these results to longer periods. To help illustrate this issue, we compute each region's rates over four overlapping five year windows, and present the results in Table S2. Some of the regions have roughly the same rates from one time span to the next. But some do not. The HMA results, especially, demonstrate that inter-annual variability can impact rates determined over short time intervals. The source of these large swings in the rates is the interannual variability evident in the Figure 2 HMA time

series. Whether the longer 8-year estimate shown in Table 1 is also significantly affected

by, in that case, decadal variability, is not clear, but we cannot rule it out.

Alaska

Our result for South Alaska shows significant mass loss (-47 ± 7 Gt/yr) during

2003-2010. This rate, though, is notably smaller than some previously published Alaska

mass loss rates from GRACE[14,37,38].   Those rates were all based on data from much

shorter data spans and from early in the mission. It is true that the Alaska mass loss rate

was larger early in the GRACE period, as can be seen from the Alaska time series shown

in Figure 2. But this effect is not large enough to completely explain our difference from

those published rates.

A related factor, though, is that when a short time span is used to infer a trend,

interannual variability can greatly impact the result. That makes the fitted trend

particularly sensitive to the hydrology correction, since hydrology signals often exhibit

large interannual variability. The final trend estimate for short data spans can thus be

critically dependent on which hydrology model is used and how that model is applied;

and those are often different in different studies. As the data span lengthens, the

correlation with interannual variability decreases and so the sensitivity to hydrology

becomes less prominent. We find, for example, that when we solve for a 2003-2007

Alaska trend, our hydrology corrections are -13 Gt/yr for GLDAS/Noah and 0 Gt/yr for

CLM4. Our results for shorter periods are even larger and more divergent: GLDAS/Noah

and CLM4 give corrections of -28 Gt/yr and -12 Gt/yr for Jan, 03 – Dec, 04, for example.

 But when solving for a 2003-2010 trend, those corrections reduce to -6 Gt/yr and -2

Gt/yr, respectively. These 8-year corrections are relatively small and in good agreement, illustrating the decreased sensitivity to the hydrology signal.

High Mountain Asia

A recent pioneering study[6] used GRACE to estimate HMA ice loss, and found a total ice change rate of -47±12 Gt/yr between April 2002 and April 2009. However, ref.[6] did not solve for separate mass variations over the adjacent plains, but simply removed groundwater at 10 Gt/yr, a rate that is only ~30 % of what we obtain by solving for mascons spread over the entire groundwater loss region. Thus, ref.[6] retained a substantial groundwater signal that was folded into the ice loss signal. Ref.[6] integrated their GRACE-minus-groundwater results over a region that included the plains (see the dashed line in Fig. 3a of ref.[6]), and adjusted the amplitude of their simulated glacier signal until it gave that same spatially integrated value. This implies that considerable groundwater loss was probably absorbed into their glacial ice solution. It must also be noted that some glacierized regions of HMA, included in this study, are exluded in ref[6], such as the Tibetan Plateau glaciers (see Fig. 3 of ref[6]).

TIBET 4 GIA model

It has been speculated there might have been a large regional ice sheet covering the entire Tibetan Plateau that melted at the end of the Pleistocene[39]. This is a controversial proposal[40,41]. Nevertheless, to see what impact such a signal might have on our results, we follow ref.[42] and consider an extreme case (model TIBET4 of ref.[42]),

where the ice is assumed to cover the entire Tibetan Plateau to an elevation of 6000 m, and to have ended its deglaciation phase 8000 years ago. We follow ref. [42] in assuming an asthenosphere viscosity of 2×10^{20} Pa-sec. We use the method described by ref. [35] to model the resulting present-day rate of change in the gravity field, and show the resulting apparent surface mass trend, smoothed with a 350-km Gaussian function, in Fig. S5. Comparing with Fig. 2d shows that although the amplitude of this hypothetical signal is of the same order as that required to offset the ref. [2] ice loss estimate, it is not centered in the same place. It does, though, lie over the glaciers in northeastern Tibet, where GRACE (Fig. 2b) sees a positive trend. Thus, although the existence of such a large late Pleistocene ice sheet is highly speculative, we have elected to break out Tibet from the rest of HMA and report it separately in Table 1, so that the result for the rest of HMA excluding Tibet is relatively free of any possible contamination from this possible GIA signal.

Erosion in HMA

We do not correct for the mass loss caused by the removal of surface rock and soil through erosional processes. In principal, this could be causing us to overestimate the HMA ice loss. Note that this omission has the wrong sign to explain the discrepancy between the GRACE HMA results and conventional estimates. In any case, we argue here that it is not likely to have a significant impact on our results.

To have an effect on a mascon solution, the eroded material must be transported outside the effective GRACE footprint (i.e. the mascon area), and not deposited within it. Thus, the most pertinent estimates of erosion rates are those based on measurements of

river sediment transport. Ref. [43] used river transport measurements to determine ongoing erosion rates for the southern Himalaya, and determined that those rates were slightly less than 10^3 ton/yr per km^2 – roughly 6 times the global average. Our total HMA mascon area is 10^6 km^2. If we assume the entire region covered by our mascons is subject to this same erosion rate, we conclude that the total HMA erosional mass loss would be only ~1 gton/yr. This is likely to be an overestimate because much of the region covered by our HMA mascons is not mountainous, and so is likely to be experiencing lower erosion rates. Furthermore, if an erosional process has been progressing at roughly the same average rate over the last tens of thousands of years or longer, it is likely to be largely isostatically compensated by relaxation in the underlying mantle (just as tectonic processes are; see the main text), at the relatively large spatial scales of GRACE.

Upscaling GIC excluding PGIC rates to obtain GIC including PGIC rates

To obtain an estimate of GIC including Greenland and Antarctica PGIC rates, we upscale our GIC excluding PGIC rates by a factor defined as the ratio between the GIC including PGIC rate to the GIC excluding PGIC rate, as determined in ref. [3]. In that study, the PGIC and GIC rates are given as 0.28 ± 0.17 mm/yr and 0.51±0.29 mm/yr, respectively. Let the ratio be f=(GIC+PGIC)/GIC=1+PGIC/GIC. If we assume the PGIC and GIC errors are uncorrelated, then the error on the scale factor is

σ_f= PGIC/GIC *sqrt($(\sigma_{PGIC}/ PGIC)^2$+$(\sigma_{GIC}/ GIC)^2$)=0.46. We thus find this factor to be f = 1.55 ± 0.46. If the errors in GIC and PGIC from ref. [3] were positively correlated, the uncertainty in the factor would be smaller than 0.46. So, in that sense, our uncertainty estimate on the scaling factor is conservative.

We propagate the errors from the scaling factor described above and from our GIC errors to obtain the GIC including PGIC estimate of -229 ± 82 Gt/yr. Similarly, the combined ice sheets mass balance is estimated at -303 ± 100 Gt/yr.

Note that this method of removing PGIC contributions from Greenland and Antarctica and adding them to GIC cannot be directly verified by the GRACE data.

Merits of GRACE and comparison to earlier studies

In our view, GRACE-based estimates of the total mass loss of a large glacial system are inherently more reliable than traditional methods that rely on the extrapolation of measurements from just a few glaciers. GRACE 'sees' the entire system. No extrapolation and no interpolation are needed. Because of its relatively coarse spatial resolution, GRACE cannot isolate individual glaciers and so cannot determine how the mass loss is partitioned between glaciers. That is where traditional techniques have the advantage. In this paper, though, we are examining entire systems.

GRACE does have limitations. The hydrology and GIA signals are the most critical potential issues, and must be removed using independent models. The challenge is to estimate reliable uncertainties associated with errors in those models, so that there is confidence the true mass loss values lie within the final error bars. Accordingly, we have spent considerable effort in this paper deriving meaningful uncertainty estimates. For every error source, we have tried to err on the conservative side when constructing those estimates.

Our HMA and total GIC results differ from some published traditional estimates, although more recent traditional measurements suggest that the GIC mass loss rate has significantly decreased after 2005 [5], reducing the difference between our results and conventionally-derived results for the same period. It is beyond the scope of this paper to try to quantify uncertainties in traditional estimates. The difficulties associated with having to determine a system-wide mass balance estimate by extrapolating measurements made on just a few glaciers, are well known in the glaciological community, and are noted in almost every paper that tries to employ those traditional methods. The estimation of the resulting errors is a serious challenge. We believe that a comparison between traditional estimates and our results can give an indication, to within our uncertainty estimates, of how large those traditional errors can be.

Supplementary References

30   Wahr, J., Molenaar, M., & Bryan, F., Time variability of the Earth's gravity field: hydrological and oceanic effects and their possible detection using GRACE. *Journal of Geophysical Research* **103**, 30,205-230,229 (1998).

31   Oleson, K.W. *et al.*, Technical Description of version 4.0 of the Community Land Model (CLM), NCAR Technical Note, NCAR/TN-478+STR, 2010.

32   Rodell, M. *et al.*, The Global Land Data Assimilation System. *Bulletin of the American Meteorological Society* **85**, 381-394 (2004).

33   Qian, T.T., Dai, A., Trenberth, K.E., & Oleson, K.W., Simulation of global land surface conditions from 1948 to 2004. Part I: Forcing data and evaluations. *Journal of Hydrometeorology* **7**, 953-975 (2006).

34   Peltier, W.R., Global glacial isostasy and the surface of the ice-age earth: The ice-5G (VM2) model and GRACE. *Annu. Rev. Earth Planet. Sci.* **32**, 111-149 (2004).

35   Paulson, A., Zhong, S.J., & Wahr, J., Inference of mantle viscosity from GRACE and relative sea level data. *Geophysical Journal International* **171**, 497-508 (2007).

36   Mann, M.E., Little Ice Age in *The Earth system: physical and chemical dimensions of global environmental change, Encyclopedia of Global Environmental Change*, edited by T. Munn (John Wiley & Sons, Ltd, Chichester, 2002), Vol. 1, pp. 504-509.

37   Chen, J., Tapley, B., & Wilson, C.R., Alaskan mountain glacial melting observed by satellite gravimetry. *Earth and Planetary Science Letters* **248** (2006).

[38]   Tamisiea, M.E., Leuliette, E.W., Davis, J.L., & Mitrovica, J.X., Constraining

hydrologi-cal and cryospheric mass flux in southeastern Alaska using space-based

gravity meas-urements. *Geophysical Research Letters* **32**, L20501 (2005).

[39]   Kuhle, M., The Pleistocene glaciation of Tibet and the onset of ice ages - An

autocycle hypothesis. *Geojournal* **17**, 581-595 (1988).

[40]   Heyman, J. *et al.*, Palaeoglaciation of Bayan Har Shan, northeastern Tibetan

Plateau: glacial geology indicates maximum extents limited to ice cap and ice

field scales. *J. Quat. Sci.* **24**, 710-727 (2009).

[41]   Owen, L.A., Caffee, M.W., Finkel, R.C., & Seong, Y.B., Quaternary glaciation of

the Himalayan-Tibetan orogen. *J. Quat. Sci.* **23**, 513-531 (2008).

[42]   Kaufmann, G., Geodetic signatures of a Late Pleistocene Tibetan ice sheet.

Journal of Geodynamics **39**, 111-125 (2005).

[43]   Chakrapani, G.J. & Saini, R.K., Temporal and spatial variations in water

discharge and sediment load in the Alaknanda and Bhagirathi Rivers in Himalaya,

India. *Journal of Asian Earth Sciences* **35**, 545-553 (2009).
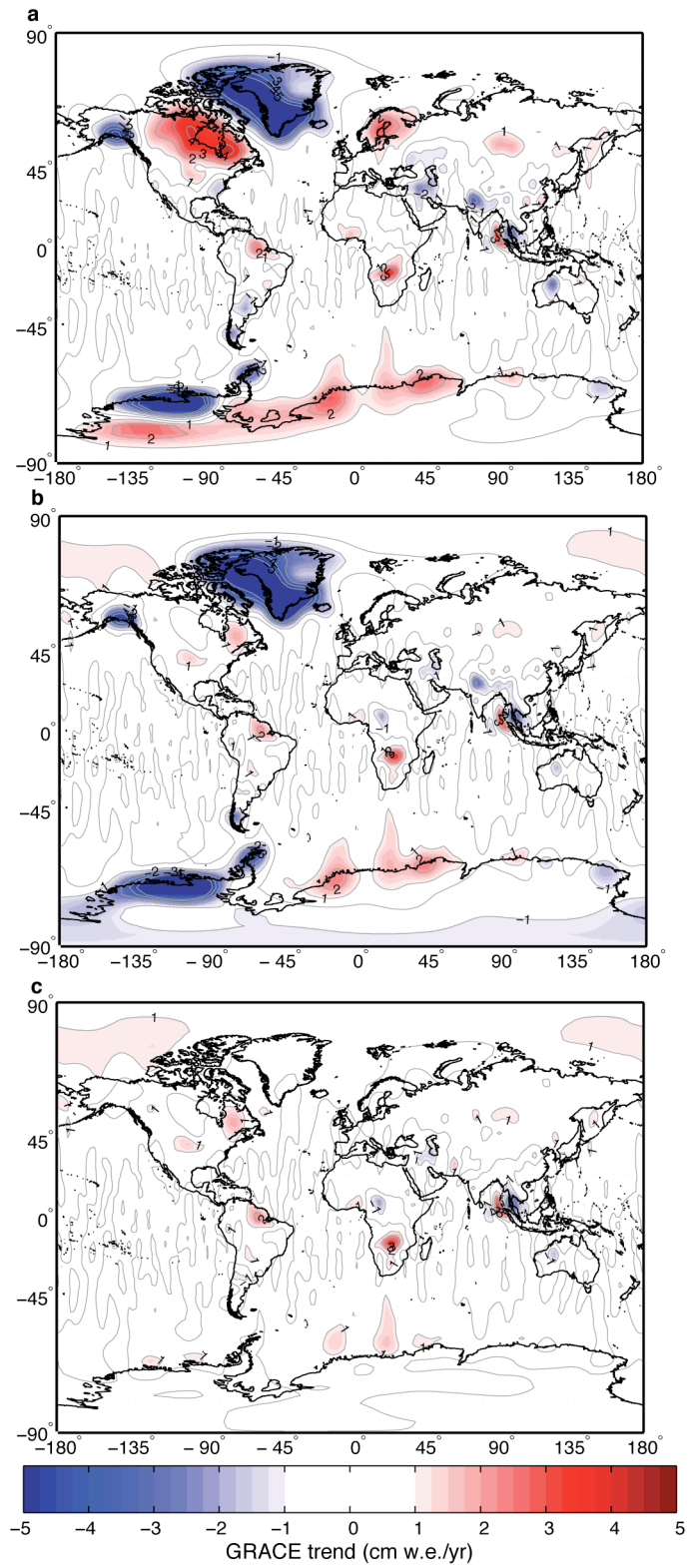
Supplementary Figures and Legends

Figure S1: Global mass trend from GRACE during 2003-2010. A 350 km Gaussian smoothing is applied. a: Grace mass trend , b: same as a, but corrected for the effects of hydrology and glacial isostatic adjustment, c: same as b, but with the inverted mascon mass estimates removed.
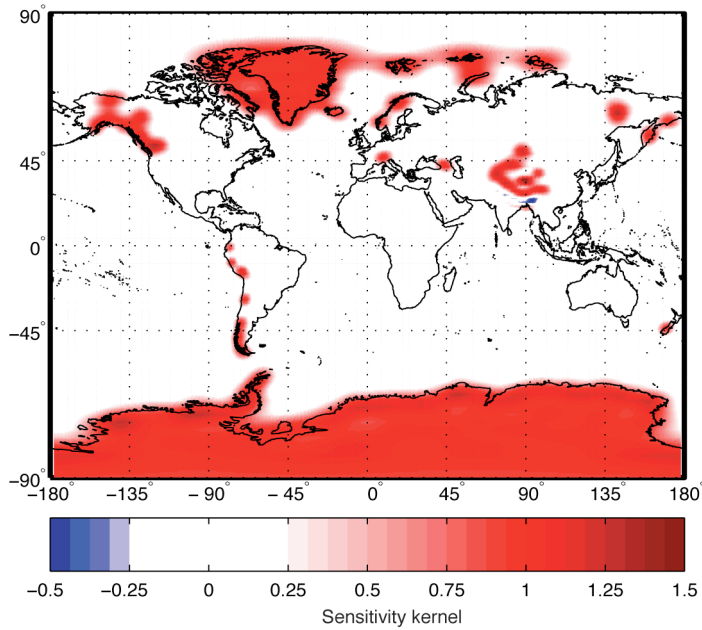

Figure S2: Sensitivity kernel for all glacierized regions represented by a mascon.
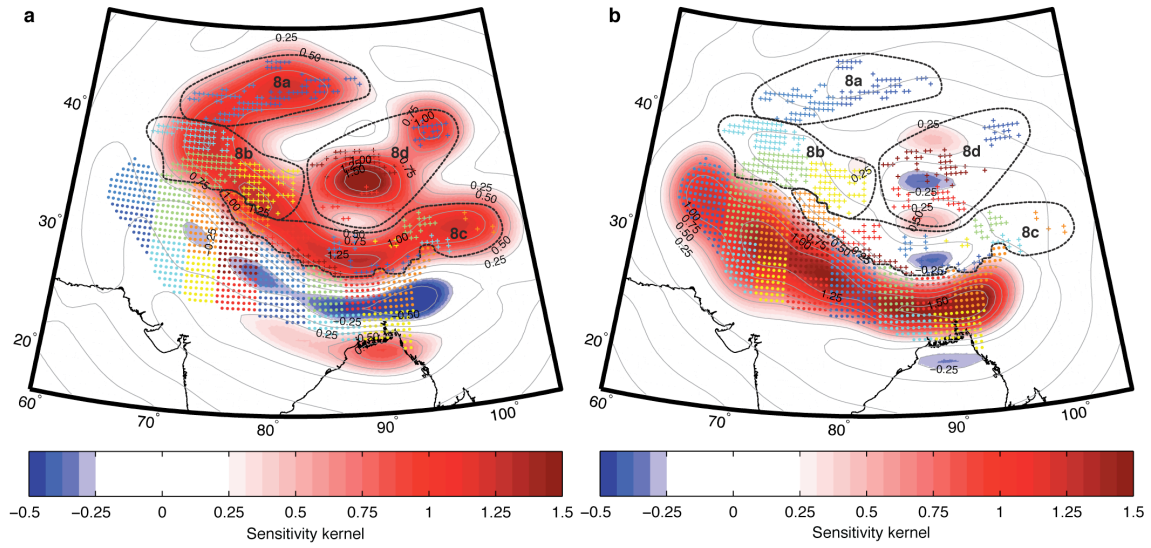
Figure S3: HMA mascons and plains mascons sensitivity kernels. a: HMA mascons sensitivity kernel, the dark-grey dashed lines delimit the boundaries between the four HMA sub regions. Colour symbols represent the mascons. b: same as a, but showing the sensitivity kernels for the plains mascons.
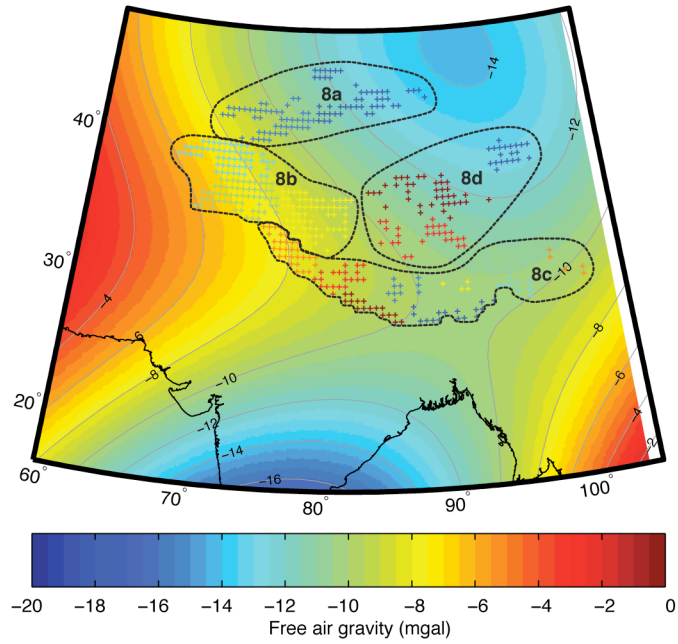
Figure S4. The static free-air gravity field over HMA from EGM96. Topographic contributions from the Himalaya and other mountainous regions are not evident, indicating a high degree of isostatic compensation.
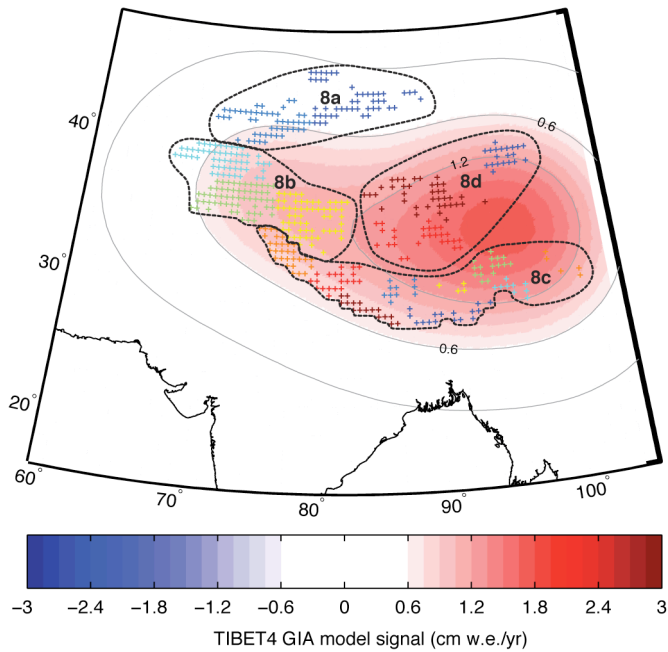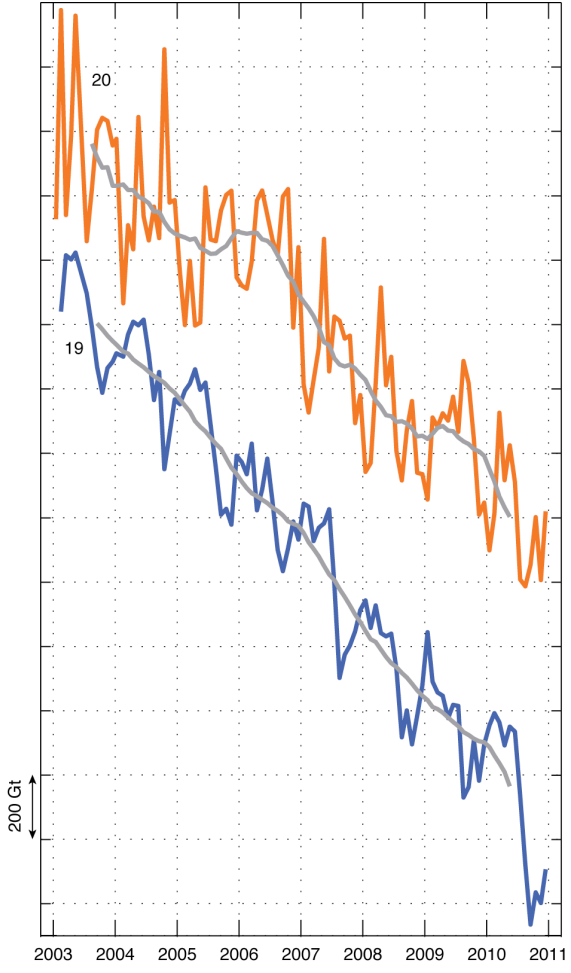

Figure S5: TIBET 4 glacial isostatic signal. HMA mascons are shown.

mass (Gt)

200 Gt

200 Gt

7

11

18

9

3

6

13

10

5

4

2

8

16

1

17

15

14

12

20

19

2003 2004 2005 2006 2007 2008 2009 2010 2011

2003 2004 2005 2006 2007 2008 2009 2010 2011
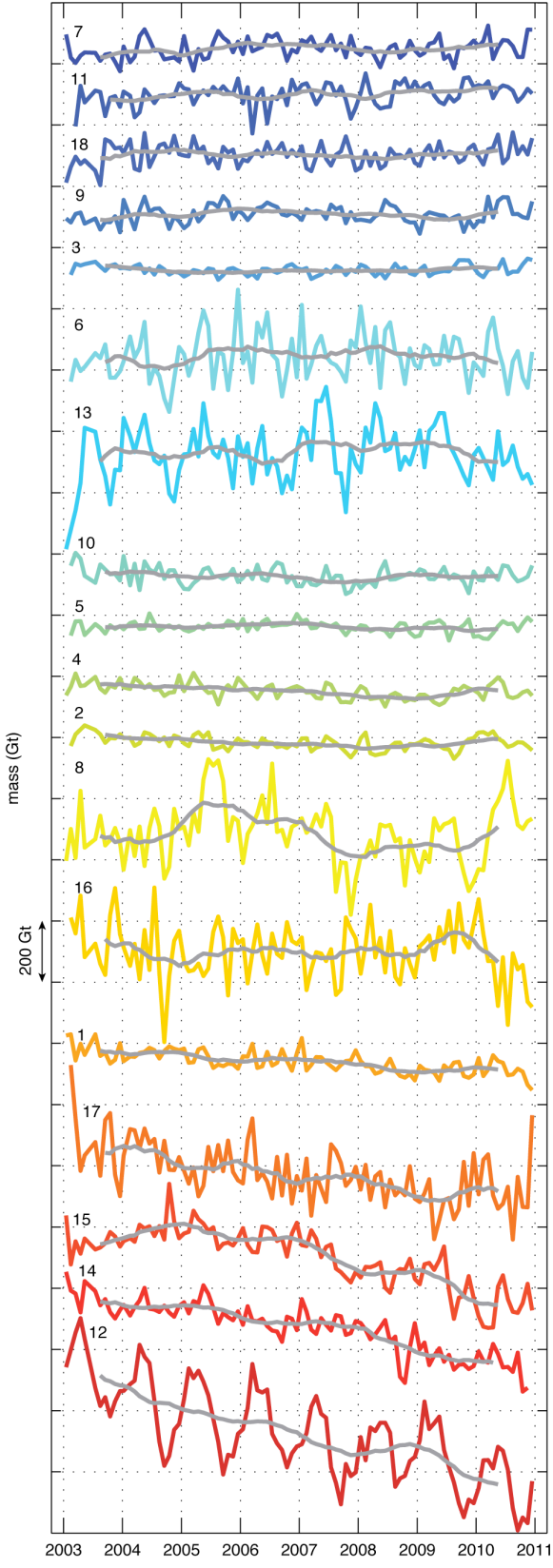
1. Iceland	11. Norway
2. Svalbard	12. Alaska
3. Franz Joseph Land	13. North America exl. Alaska
4. Novaya Zemlya	14. Baffin Island
5. Severnaya Zemlya	15. Ellesmere and Devon Islands
6. Siberia and Kamtchatka	16. South America excl. Patagonia
7. Altai	17. Patagonia
8. High Mountain Asia	18. New Zealand
9. Caucasus	19. Greenland IS + PGIC
10. Alps	20. Antarctica IS + PGIC

Figure S6: Mass change during 2003-2010 for all mascon regions shown in Fig. 1 and Table 1. The grey lines represent a 13-month window low pass filtered version of the data. Time series are shifted for legibility. Modelled contributions from GIA, LIA, and hydrology have been removed. Similar to Figure 2, but Greenland + PGIC and Antarctica + PGIC are also included.

Supplementary Tables

	Mass balance rate	GRACE only	GIA correction	LIA correction	Hydrology correction
1. Iceland	-11±2	-10±2	0±0	0±0	0±0
2. Svalbard	-3±2	-1±2	-1±1	0±0	0±0
3. Franz Josef Land	0±2	3±1	-2±1	0±0	0±0
4. Novaya Zemlya	-4±2	-1±2	-3±1	0±0	0±0
5. Severnaya Zemlya	-1±2	0±2	0±0	0±0	0±0
6. Siberia and Kamchatka	2±10	1±7	-1±1	0±0	3±7
7. Altai	3±6	2±3	-1±0	0±0	2±6
8. High Mountain Asia	-4±20	-10±9	-7±3	-3±1	16±17
8a. Tianshan	-5±6	-10±3	-1±1	0±0	6±5
8b. Pamirs and Kunlun Shan	-1±5	-3±4	-1±1	-1±0	3±1
8c. Himalaya and Karakoram	-5±6	-7±5	-2±1	-1±1	5±4
8d. Tibet and Qilian Shan	7±7	8±4	-2±1	-1±0	1±6
9. Caucasus	1±3	1±2	0±0	0±0	0±1
10. Alps	-2±3	1±3	0±0	0±0	-3±1
11. Scandinavia	3±5	9±4	-6±3	0±0	0±2
12. Alaska	-46±7	-43±5	0±0	-7±4	4±4
13. Northwest America excl. S. Alaska	5±8	5±7	-3±2	0±0	4±3
14. Baffin Island	-33±5	-27±4	-6±3	0±0	-1±1
15. Ellesmere, Axel Heiberg and Devon Islands	-34±6	-27±5	-6±3	0±0	0±0
16. South America excl. Patagonia	-6±12	-10±8	-2±1	0±0	6±9
17. Patagonia	-23±9	-13±7	-2±1	-9±5	0±3
18. New Zealand	2±3	2±3	0±0	0±0	0±1
19. Greenland ice sheet + PGIC	-222±9	-227±7	5±-2	0±0	1±5
20. Antarctica ice sheet + PGIC	-165±72	-23±16	-141±71	0±0	-1±1
total	-536±93	-370±26	-178±89	-19±9	31±9
Glaciers and Ice caps excl. Greenland and Antarctica PGIC	-148±30	-119±19	-42±21	-19±9	31±4
Antarctica + Greenland ice sheet and PGIC	-384±71	-248±17	-136±68	0±0	0±6

Table S1: Inverted mass balance rates and their constitutive elements for each glacierized region between January 2003 and December 2010. GRACE-only uncertainties are given at the two-sigma level. Other uncertainties are estimated as described in the text.

	Jan 03-Dec 07	Jan 04-Dec 08	Jan 05-Dec 09	Jan 06-Dec 10	Jan 03-Dec 10
1. Iceland	-10±5	-12±4	-11±5	-11±5	-11±2
2. Svalbard	-10±3	-6±3	-3±4	2±4	-3±2
3. Franz Josef Land	-4±3	-1±3	3±3	3±3	0±2
4. Novaya Zemlya	-7±4	-9±4	-7±4	-1±4	-4±2
5. Severnaya Zemlya	1±3	-3±3	-2±3	-3±3	-1±2
6. Siberia and Kamchatka	9±15	9±17	-3±15	-5±15	2±10
7. Altai	8±8	0±6	-2±6	1±9	3±6
8. High Mountain Asia	-2±20	-16±19	-37±18	2±36	-4±20
8a. Tianshan	-5±5	-9±4	-15±5	-5±13	-5±6
8b. Pamirs and Kunlun Shan	-5±10	-8±9	-11±8	4±9	-1±5
8c. Himalaya and Karakoram	-3±12	-2±10	-14±11	-9±16	-5±6
8d. Tibet and Qilian Shan	6±10	2±10	2±8	11±8	7±7
9. Caucasus	5±5	-2±5	-6±4	-2±4	1±3
10. Alps	-7±6	-5±5	0±5	2±5	-2±3
11. Scandinavia	-1±10	3±9	1±8	4±7	3±5
12. Alaska	-56±16	-41±11	-40±10	-46±12	-46±7
13. Northwest America excl. S. Alaska	17±22	7±13	7±13	-2±17	5±8
14. Baffin Island	-21±7	-24±7	-40±9	-42±10	-33±5
15. Ellesmere, Axel Heiberg and Devon Islands	-12±9	-33±8	-42±8	-53±10	-34±6
16. South America excl. Patagonia	-13±21	-4±16	10±26	-8±33	-6±12
17. Patagonia	-29±15	-26±13	-23±15	-21±17	-23±9
18. New Zealand	2±7	-5±6	-1±5	3±5	2±3
19. Greenland ice sheet + PGIC	-199±14	-228±16	-230±15	-230±16	-222±9
20. Antarctica ice sheet + PGIC	-138±77	-170±77	-167±76	-195±76	-165±72
total	-480±108	-566±109	-592±106	-591±102	-536±93
Glaciers and Ice caps excl. Greenland and Antarctica PGIC	-106±57	-168±54	-196±48	-159±43	-148±30
Antarctica + Greenland ice sheet and PGIC	-351±76	-398±76	-397±75	-426±76	-384±71
Total contribution to SLR	-1.33±0.30	-1.56±0.30	-1.63±0.29	-1.63±0.28	-1.48±0.26
GIC excl. Greenland and Antarctica PGIC SLR	-0.29±0.16	-0.46±0.15	-0.54±0.13	-0.44±0.12	-0.41±0.08
Antarctica + Greenland ice sheet and PGIC SLR	-0.97±0.21	-1.10±0.21	-1.09±0.21	-1.17±0.21	-1.06±0.19

Table S2: Inverted mass balance rates for each ice-covered region for five consecutive overlapping five-year time periods. Uncertainties are given at the 95% (2 sigma) confidence level. The last column shows Table 1 results for comparison purposes.